Journal of Materials Chemistry C

PAPER

View Article Online
View Journal | View Issue

Cite this: J. Mater. Chem. C, 2018, 6, 7652

Synchronously improved dielectric and mechanical properties of wave-transparent laminated composites combined with outstanding thermal stability by incorporating iysozyme/POSS functionalized PBO fibers

Junwei Gu, *[ab] Yang Li,[a] Chaobo Liang,[a] Yusheng Tang,[a] Lin Tang,[a] Yikun Zhang,[a] Jie Kong, [a] Hu Liu [cd] and Zhanhu Guo *[c]

Modified bisphenol A dicyanate ester (m-BADCy) wave-transparent laminated composites reinforced with functionalized poly(*p*-phenylene-2,6-benzobisoxazole) (f-PBO) fibers were fabricated using an optimized method of impregnation-winding followed by lamination-molding. m-BADCy was synthesized from copolymerization between (2-((3-trifluoromethyl)phenoxy)methyl)oxirane and the BADCy matrix. f-PBO fibers were obtained by modifying with lysozyme followed by polyhedral oligomericsilsesquioxane (POSS). Lysozyme was coated on the surface of PBO fibers (PBO@lysozyme) and polyhedral oligomericsilsesquioxane (POSS) was grafted onto the PBO@lysozyme fibers (POSS-*g*-PBO@lysozyme, f-PBO fibers). The dielectric constant (ε), 2.81, and dielectric loss ($\tan\delta$), 0.0028, for f-PBO fiber/m-BADCy wave-transparent laminated composites were lower than those of PBO fiber/m-BADCy wave-transparent laminated composites (ε = 2.91 and $\tan\delta$ = 0.0043). The interlaminar shear strength (ILSS) and the flexural strength of the f-PBO fiber/m-BADCy wave-transparent laminated composites were significantly increased to 47.6 and 805.8 MPa, increased by 23.0% and 33.5% in comparison to those of PBO fiber/m-BADCy wave-transparent laminated composites (ILSS = 38.7 MPa and flexural strength = 603.5 MPa), respectively. In addition, the corresponding heat resistance index (T_{HRI}, representing thermal stability) and glass transition temperature (T_g) of the f-PBO fiber/m-BADCy wave-transparent laminated composites were 228.3 and 252.1 °C, respectively.

Received 16th May 2018,
Accepted 18th June 2018

DOI: 10.1039/c8tc02391c

rsc.li/materials-c

1. Introduction

Fiber-reinforced polymeric matrix composites possess the advantages of light weight, high specific strength & modulus, good fatigue resistance, *etc.*, and have been widely used in the aerospace industry and military fields.[1–5] With the increasing requirements for new generation weaponry (light weight, high structural load, excellent electronic warfare capability and low radar cross-sectional area), high quality wave-transparent polymeric composites with comprehensive properties (broad-band, low loss, high-temperature resistance, heat & humidity resistance and excellent mechanical properties, *etc.*) urgently need to be designed and fabricated.[6–9]

At present, common reinforcing fibers mainly include glass fibers,[10] quartz fibers,[11] Kevlar fibers,[12] carbon fibers,[13] and ultrahigh molecular weight polyethylene (UHMWPE) fibers,[14] *etc.* Though quartz fibers can usually meet the broad-band wave-transparency performance requirement of radar covers, they still cannot satisfy the light weight requirement owing to their too high density.[15] Compared to quartz fibers, poly(*p*-phenylene-2,6-benzobisoxazole) (PBO) fibers possess a relatively lower density (1.56 g cm^{-3}), outstanding dielectric properties (ε = 3.0 and $\tan\delta$ = 0.001),[16,17] more prominent mechanical properties (a tensile strength of 5.8 GPa and a tensile modulus of 270 GPa),[18,19] and outstanding heat resistance,[20] making them promising for applications in key areas of aerospace, navigation,

[a] MOE Key Laboratory of Material Physics and Chemistry under Extraordinary Conditions, Shaanxi Key Laboratory of Macromolecular Science and Technology, Department of Applied Chemistry, School of Science, Northwestern Polytechnical University, Xi'an, Shaanxi, 710072, P. R. China. E-mail: nwpugjw@163.com, gjw@nwpu.edu.cn
[b] Institute of Intelligence Material and Structure, Institute of Unmanned Systems, Northwestern Polytechnical University, Xi'an, Shaanxi, 710072, P. R. China
[c] Integrated Composites Laboratory (ICL), Department of Chemical & Biomolecular Engineering, University of Tennessee, Knoxville, TN37996, USA. E-mail: nanomaterials2000@gmail.com, zguo10@utk.edu
[d] National Engineering Research Center for Advanced Polymer Processing Technology, Zhengzhou University, Zhengzhou, 450002, P. R. China

and bulletproof and reinforced materials, especially for wave-transparent polymeric composites with light weight and high-strength.[21,22] Nevertheless, the surface of PBO fibers is highly chemically inert, and the interfacial adhesion of PBO fibers to the polymeric matrix is very weak, which severely restricts their applications in new generation weaponry.[23–26] At present, the interfacial compatibility for polymeric composites was mainly improved by surface functionalization of PBO fibers. Common methods mainly include physical modifications by plasma[27,28] and ion beam irradiation;[29] and chemical modification (such as oxidation treatment,[30,31] coupling agent modification,[32] *etc.*). These methods can make the PBO fiber surface rougher or introduce reactive functional groups on the surface of PBO fibers, but these also inevitably damage the mechanical properties of PBO fibers themselves.[33,34]

Lysozyme is a kind of natural protein with an amyloid structure,[35,36] which can form insoluble aggregates or two-dimensional nano-films on the substrate surfaces. Certainly, lysozyme also presents the advantages of good colorless transparency, biocompatibility and controllable degradation.[37–39] Therefore, inspired by stable adhesion of the amyloid structure, the lysozyme phase transition assembly should be fast, mild and present stable adhesion to all kinds of material surfaces. In addition, it can also introduce some chemically active sites (amino, hydroxyl and carboxyl groups) to be further modified.[40–42] Polyhedral oligomeric silsesquioxane (POSS) presents excellent dielectric properties, thermal stability and special surface performance.[43–45] The introduction of POSS on the surface of PBO fibers *via* chemical bonding might solve the problem of poor interfacial compatibility between PBO fibers and the polymeric matrix,[46] in favor of improving the mechanical properties of polymeric composites. Meanwhile, the dielectric properties of the composites can also be further improved by incorporating the unique structure of POSS.

In comparison to other thermosetting resins, such as epoxy resin,[47,48] polyimide,[49,50] phenolic resin[51] and bimaleimide resin,[52] *etc.*, cyanate ester (CE) resin possesses a relatively lower dielectric constant (ε = 2.6–3.2)[53–55] and dielectric loss tangent ($\tan\delta$ = 0.002–0.008).[56–58] Furthermore, CE presents excellent mechanical properties, good moisture resistance & thermal stability, and high dimensional stability. CE has been thus widely used in radomes and satellite antenna systems.[59–61] However, the relatively lower toughness and interlaminar shear strength (ILSS) of the cured pure CE resins have limited their wider applications.[62–64]

In the present work, novel functionalized PBO fiber/modified bisphenol A dicyanate ester (f-PBO fiber/m-BADCy) wave-transparent laminated composites were designed and fabricated with excellent comprehensive properties using an optimized method of impregnation-winding followed by lamination-molding. Herein, m-BADCy was fabricated from the copolymerization between (2-((3-trifluoromethyl)phenoxy)methyl) oxirane and the BADCy matrix according to our previous work,[65] and f-PBO fibers were also obtained by grafting lysozyme followed by epoxycyclohexyllsobutyl polyhedral oligomeric silsesquioxane (POSS). The effects of surface functionalization on the surface morphologies, structures and properties of the PBO fibers were analyzed, and the corresponding functionalization mechanism was also deduced based on analyses using Fourier transform infrared spectroscopy (FTIR), X-ray photoelectron spectroscopy (XPS), thermogravimetric analysis (TGA), and scanning electron microscopy (SEM). Furthermore, the content and surface functionalization effects of the PBO fibers on the dielectric & mechanical properties and thermal stabilities of the f-PBO fiber/m-BADCy wave-transparent laminated composites were also investigated.

2. Experimental

2.1. Main materials

Bisphenol A dicyanate ester (BADCy), with a relative molecular weight of 278.32 g mol^{-1}, was purchased from Wuqiao Resin of Jiangsu Factory Co. Ltd (Jiangsu, China). Poly(*p*-phenylene-2,6-benzobisoxazole) (PBO) fibers were supplied by Toyobo Co. Ltd (Osaka, Japan). *m*-(Trifluoromethyl)phenol ($\geq$99%) was obtained from Aladdin Reagent Co. Ltd (Shanghai, China). Epichlorohydrin ($\geq$99%) was purchased from TCI Development Co. Ltd (Tokyo, Japan). Dichloromethane was received from Tianjin Chemical Reagent Co. Ltd (Tianjin, China). Potassium carbonate was bought from Kermel Chemical Reagent Co. Ltd (Tianjin, China). Dibutyltin dilaurate (DBTDL) was supplied by Alfa Aesar Chemical Co. Ltd (Tianjin, China). Anhydrous ethanol (EtOH) and tetrahydrofuran (THF) were both purchased from Tianjin Fuyu Fine Chemical Co. Ltd (Tianjin, China). Tris(2-carboxyethyl)phosphine (TCEP) was supplied by Suzhou Haofan Biological Co. Ltd (Jiangsu, China). Lysozyme was obtained from Beijing Solaibao Technology Co. Ltd (Beijing, China). Epoxycyclohexyllsobutyl polyhedral oligomeric silsesquioxane (EP-POSS) was received from Hybrid Plastics Co. Ltd (California, America).

2.2. Surface functionalization of PBO fibers

PBO fibers were firstly purified by soaking in EtOH and THF in sequence for 12 hours, and then dried in a vacuum oven at 80 °C for 12 hours before use. Lysozyme solution with a concentration of 2 mg mL^{-1} was obtained by dissolving lysozyme in distilled water. The TCEP buffer solution with a concentration of 5 $\times$ 10^{-3} mol L^{-1} was also prepared (pH = 6.0). Then the above pre-purified PBO fibers were immediately immersed in the following mixed solution (TCEP/lysozyme = 1/1, vol/vol) for 2 hours, washed with distilled water, and then dried in a vacuum oven at 30 °C for another 12 hours, to finally obtain the lysozyme modified PBO (PBO@lysozyme) fibers. In addition, the obtained PBO@lysozyme fibers were then immersed in the POSS/THF solution with a concentration of 0.5 wt% at 40 °C for 6 hours and washed with distilled water, and then dried in the vacuum oven at 80 °C for another 12 hours, finally to obtain the POSS functionalized PBO (POSS-*g*-PBO@lysozyme, f-PBO) fibers. The process for functionalizing PBO (f-PBO) fibers was schematically presented in Fig. 1.

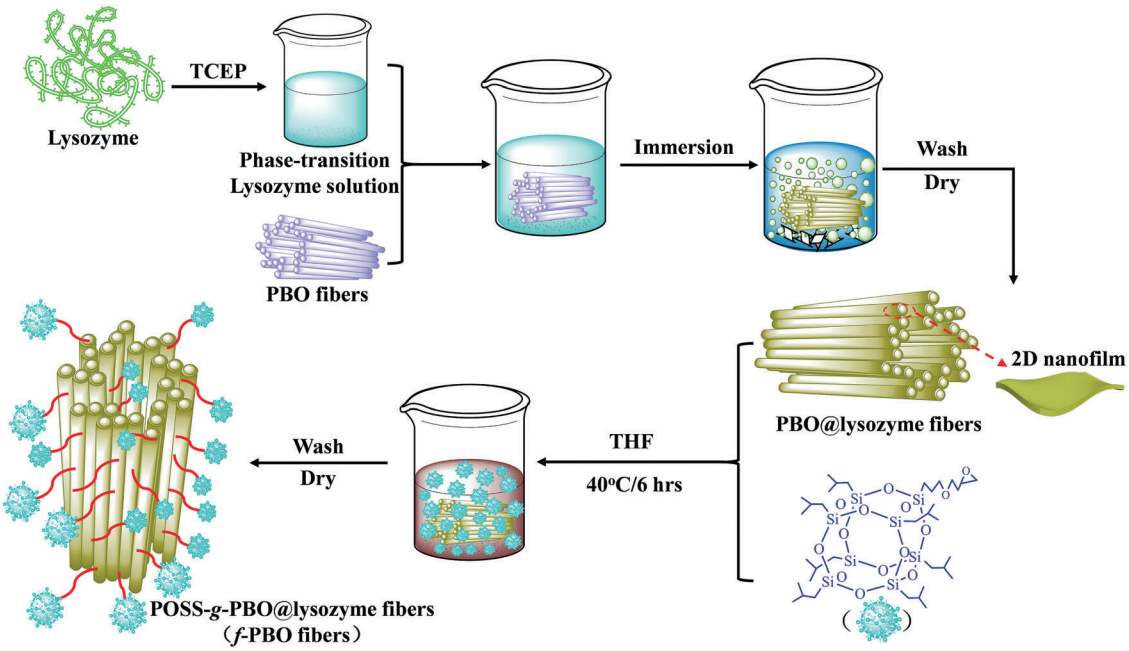

Fig. 1 Schematic diagram of the general fabrication process of functionalized PBO (f-PBO) fibers.

2.3 Fabrication of PBO fiber/m-BADCy wave-transparent composites

m-BADCy was firstly prepolymerized at 150 °C for 4 hours, then cooled down to 80 °C, followed by the addition of excessive acetone and the appropriate amount of DBTDL, to finally obtain the prepreg glue. The PBO fibers were then immersed in the above prepreg glue, followed by wet-winding and air-drying procedures to obtain the PBO fiber/m-BADCy mixtures. The above PBO fiber/m-BADCy prepregs (three layers) were laid up according to unidirectional lamination, then laminated and hot pressed under non-vacuum conditions at 10 MPa according to the following conditions: 160 °C/1 h + 180 °C/2 h + 200 °C/5 h, followed by post-curing at 220 °C for another 2 h. Finally, the corresponding m-BADCy wave-transparent composites (200 mm × 100 mm × 2 mm) were obtained successfully.

2.4 Characterization

Fourier transform infrared (FTIR) spectra of the samples were obtained using Bruker Tensor 27 equipment (Bruker Corp., Germany). X-ray photoelectron spectroscopy (XPS) analyses of the samples were carried out using K-Alpha equipment (Thermoelectric Corp., America). Thermal gravimetric (TG) analyses of the samples were performed at a heating rate of 10 °C min^{-1} (argon atmosphere) over the whole range of temperature (40–800 °C) using a STA 449F3 (NETZSCH C Corp., Germany). Dynamic mechanical analyses (DMA) of the samples were measured at 5 °C min^{-1} at 1 Hz over the whole range of temperature (25–300 °C) by means of a Q800 (TA Instruments Corporation, America). Dielectric constant (ε) and dielectric loss tangent ($\tan\delta$) values of the samples were measured using a Novocontrol Technologies Alpha-A high-resolution dielectric analyzer (Novocontrol Corp., Germany) at room temperature, and the corresponding specimen dimensions were 20 mm × 20 mm × 2 mm. Scanning electron microscopy (SEM) morphologies of the samples were analyzed using a VEGA3-LMH (TESCAN Corp., Czech Republic). The flexural strength and the interlaminar shear strength (ILSS) of the samples were measured using an electron omnipotence experiment machine SANS-CMT5105 (Shenzhen New Sansi Co., China) according to ASTMD 7264-2007 and ASTMD 2344-2000, respectively. The single fiber pull-out test was performed using the single fiber electronic tensile strength tester YM-06B (Laizhou Yuanmao Instrument Co., China), and 30 specimens were tested to obtain the average value for the single fiber pull-out strength of the PBO fibers.

3. Results and discussion

3.1. PBO, PBO@lysozyme and f-PBO fibers

Fig. 2 shows the FTIR spectra of pristine PBO, PBO@lysozyme and f-PBO fibers. The band at 1620, 1500 and 3058 cm^{-1} for

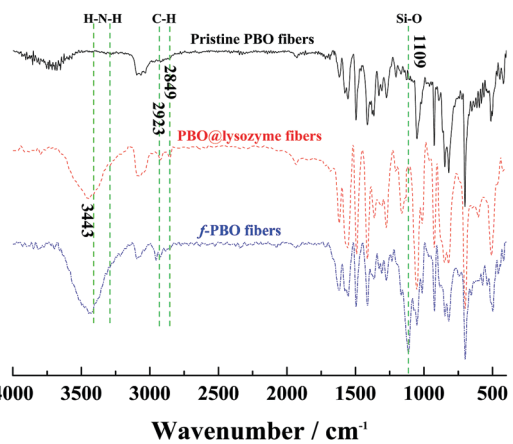

Fig. 2 FTIR spectra of the pristine PBO, PBO@lysozyme and f-PBO fibers.

pristine PBO fibers could be assigned to the stretching vibration of C=C, C–C and C–H for the benzene ring, respectively.[66] The band at 1050 cm^{-1} could be attributed to the characteristic peak of C–O–C for the oxazole ring. For the PBO@lysozyme fibers, the bands at 2923 and 2849 cm^{-1} were assigned to the characteristic peaks of aliphatic C–H groups in lysozyme. In addition, the observed new double absorption peaks at 3300–3500 cm^{-1} and at 3443 cm^{-1} could be attributed to the characteristic absorption of the primary amine ($-NH_2$) and O–H of lysozyme, respectively. For the f-PBO fibers, the double absorption peak at 3300–3500 cm^{-1} (primary amine, $-NH_2$) changed into a single absorption peak (secondary amine, –NH–), ascribed to the reaction of the epoxy group in POSS and the NH_2 group in lysozyme. Meanwhile, a new characteristic absorption peak of Si–O also appeared at 1109 cm^{-1}.

Fig. 3 shows the XPS spectra of the pristine PBO, PBO@lysozyme and f-PBO fibers, and the corresponding results calculated using the sensitivity factor are also listed in Table 1. A certain amount of carbon, oxygen and nitrogen elements were noticed on the surface of pristine PBO fibers. For the PBO@lysozyme fibers, sulfur element was observed, the concentration of C element also decreased significantly, and the concentrations of O and N elements both increased. Compared to those of PBO@lysozyme fibers, the concentrations of C, N and S elements for f-PBO fibers all decreased, and the concentration of O element increased. In addition, the new peak of Si also appeared. It was mainly ascribed to the contribution of oxygen and silicon of POSS.

Fig. 4 shows the TGA curves of the pristine PBO, PBO@lysozyme and f-PBO fibers. For pristine PBO fibers, the weight loss was less than 1% below 100 °C, mainly ascribed to the loss of adsorption water and small molecules on the surface of PBO fibers. At 900 °C, the corresponding weight loss of pristine PBO fibers reached 34.1%, attributed to the decomposition of PBO fibers at higher temperatures. For PBO@lysozyme and f-PBO fibers, the corresponding weight loss increased obviously with increasing the temperature. Such differences were mainly attributed to the fact that both the lysozyme and POSS were oxidized and decomposed at higher temperatures. Fig. 5 presents the SEM morphologies of the pristine PBO, PBO@lysozyme and f-PBO fibers. Pristine PBO fibers presented smooth surfaces with a mean diameter of ~11.4 μm. Compared with pristine PBO fibers, both PBO@lysozyme and f-PBO fibers became rougher. Meanwhile, the corresponding mean diameter also increased to 12.6 μm (PBO@lysozyme fibers) and 13.2 μm (f-PBO fibers), respectively. FTIR, XPS, TGA and SEM analyses revealed that lysozyme was coated onto the surface of PBO fibers and POSS was also successfully grafted onto the PBO@lysozyme fibers.

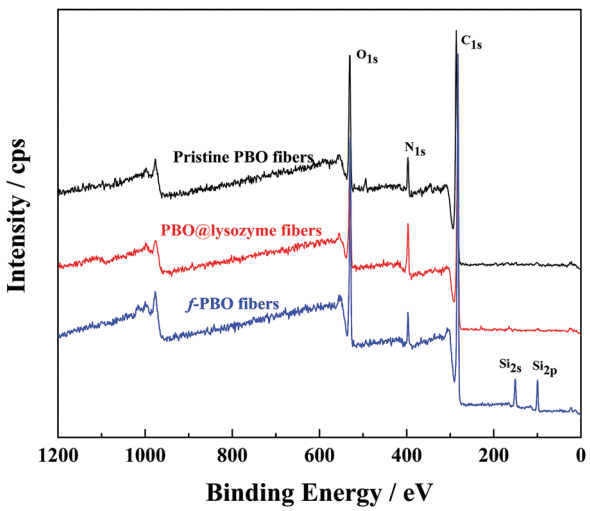

Fig. 3 XPS spectra of the pristine PBO, PBO@lysozyme and f-PBO fibers.

Table 1 Concentrations of various elements on the PBO fibers' surface

Samples	Concentrations of various elements/%				
	C	N	O	S	Si
Pristine PBO fibers	79.35	6.63	14.02	—	—
PBO@lysozyme fibers	75.75	8.70	15.11	0.44	—
f-PBO fibers	71.71	5.20	17.27	0.16	5.66

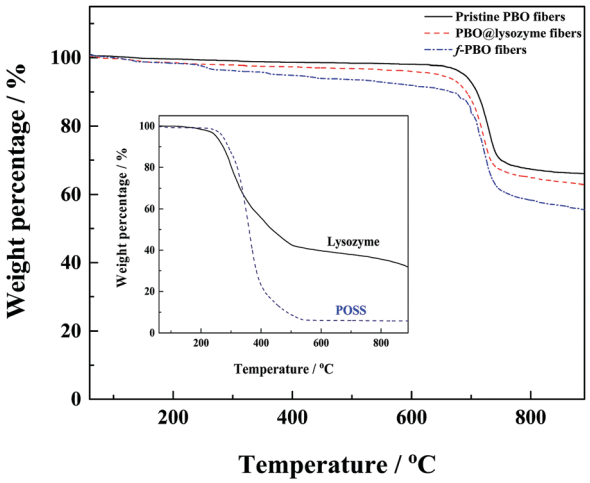

Fig. 4 TGA curves of the pristine PBO, PBO@lysozyme and f-PBO fibers.

3.2. PBO fiber/m-BADCy micro-composites

Fig. 6 shows the single fiber pull-out strength and the corresponding SEM images of the pristine PBO, PBO@lysozyme and f-PBO fibers. Compared with that of the pristine PBO fiber/m-BADCy micro-composites (3.21 MPa), the single fiber pull-out strength of the PBO@lysozyme fiber/m-BADCy and f-PBO fiber/m-BADCy micro-composites increased to 3.73 and 4.00 MPa, respectively. The reason was that the surface of pristine PBO fibers was smooth (insert a), presenting relatively poorer interfacial bonding to the m-BADCy matrix. For the PBO@lysozyme and f-PBO fibers, new combined layers between functionalized PBO fibers and the m-BADCy matrix were formed (insert b and c, both PBO@lysozyme and f-PBO fibers presented obvious grooves and some residual m-BADCy resin appeared on the functionalized fiber surface), ascribed to the introduced lysozyme and POSS, which would be in favor of improving the interfacial bonding of PBO@lysozyme and f-PBO fibers to the m-BADCy matrix. Furthermore, the tensile modulus and strength values (Table 2) of pristine and functionalized PBO

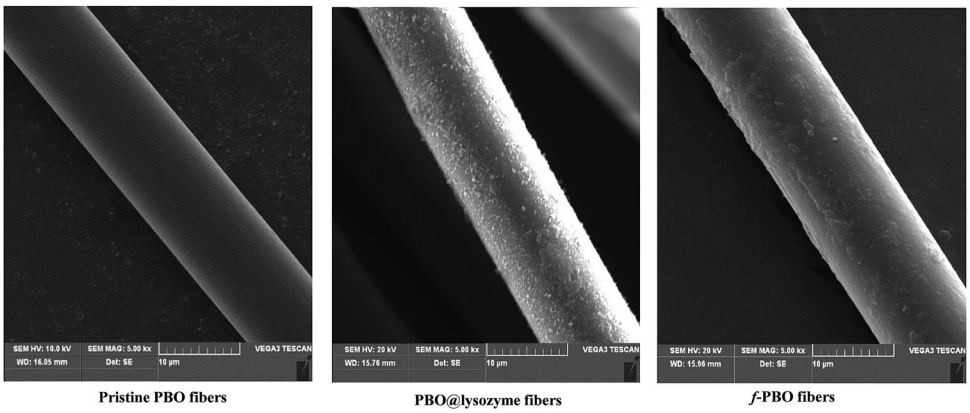

Fig. 5 SEM morphologies of the pristine PBO, PBO@lysozyme and f-PBO fibers.

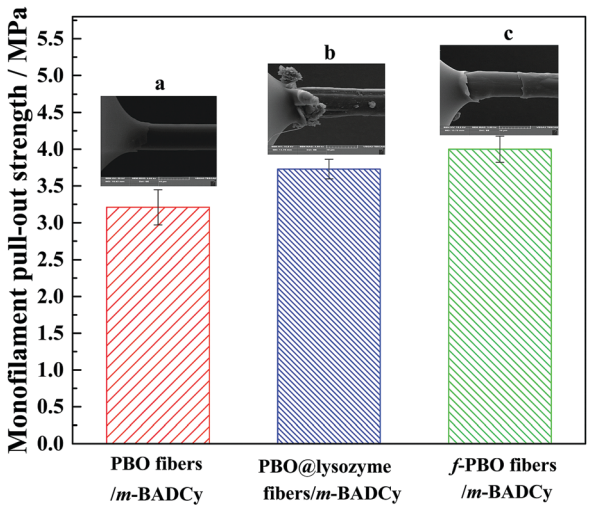

Fig. 6 Single fiber pull-out strength and the corresponding SEM images of the pristine PBO, PBO@lysozyme and f-PBO fibers.

Table 2 Tensile modulus and strength values of pristine and functionalized PBO fibers

Samples	Tensile modulus/GPa	Tensile strength/GPa
Pristine PBO fibers	40.01	1.69
PBO@lysozyme fibers	41.81	1.72
f-PBO fibers	40.17	1.70

fibers also revealed that the surface functionalization improved the tensile properties of the PBO fibers slightly.

3.3. PBO fiber/m-BADCy wave-transparent laminated composites

3.3.1. Dielectric properties. Fig. 7 presents the ε and $\tan\delta$ values of the PBO fiber/m-BADCy wave-transparent laminated composites at different testing frequencies. Compared with those of pristine PBO fiber/m-BADCy and PBO@lysozyme fiber/m-BADCy wave-transparent laminated composites, the f-PBO fiber/m-BADCy wave-transparent laminated composites possessed better dielectric properties at the same test frequency. The ε and $\tan\delta$ values at 10^7 Hz decreased to 2.81 and 0.0028, reduced by 3.4% and 34.9% in comparison to those of pristine PBO fiber/m-BADCy wave-transparent laminated composites (ε = 2.91 and $\tan\delta$ = 0.0043), respectively. The reason was that the interfacial compatibilities between PBO@lysozyme fibers, f-PBO fibers and the m-BADCy matrix were effectively improved, beneficial to the transportation of charges, thus reducing the interfacial polarization effects. Meanwhile, the introduction of POSS could further improve the dielectric properties of the f-PBO fiber/m-BADCy wave-transparent laminated composites owing to their fairly lower polar Si–O bond and unique inorganic nanocavity structure.

With increasing the test frequency, the ε values of the pristine PBO fiber/m-BADCy, PBO@lysozyme fiber/m-BADCy and f-PBO fiber/m-BADCy wave-transparent laminated composites all decreased. But the corresponding $\tan\delta$ value firstly increased and then decreased. The reason was that the electronic, atomic, interfacial and orientation polarization could completely keep up with the electric field changes under a relatively low frequency electric field ($<10^5$ Hz), resulting in a relatively higher ε value and a lower $\tan\delta$ value. With increasing the test frequency (10^5–10^7 Hz), the dipoles could keep up with the changes of electric fields but could not absolutely adapt to such changes, and the friction resistance of the dipole orientation must be overcome to generate heat. At the relatively higher frequency region ($>10^7$ Hz, Debye dispersion equation[67]), electronic and atomic polarization could only follow the changes of the electric fields, resulting in lower ε and $\tan\delta$ values.

During the propagation of electromagnetic waves, the relationships for energy loss (A), reflection coefficient (Γ), and wave transmission efficiency (T) are listed as eqn (1)–(3):[68]

$$A = \frac{2\pi d\varepsilon \tan\delta}{\lambda(\delta - \sin^2\theta)^{1/2}} \quad (1)$$

$$\Gamma = \frac{(\varepsilon - \sin^2\theta)^{1/2} - \varepsilon\cos\theta}{(\varepsilon - \sin^2\theta)^{1/2} + \varepsilon\cos\theta} \quad (2)$$

$$|T|^2 = 1 - A - |\Gamma|^2 \quad (3)$$

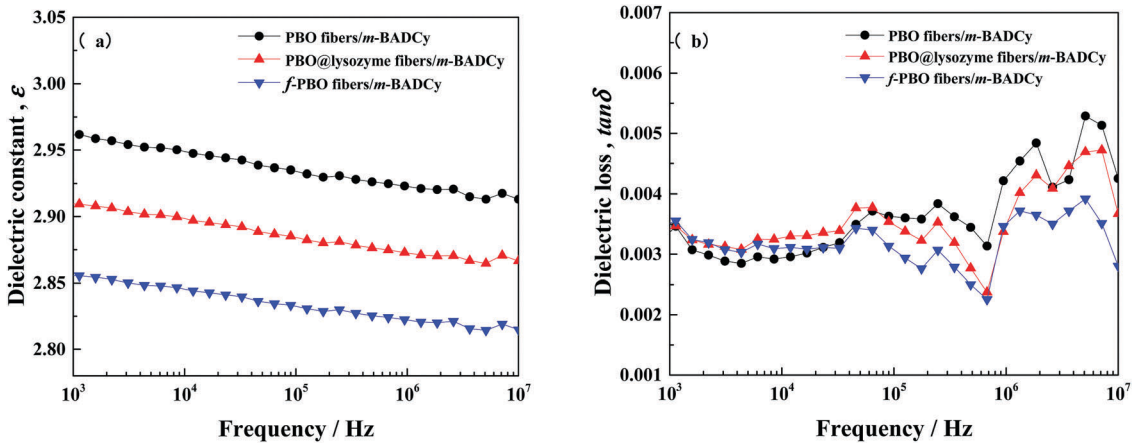

Fig. 7 ε (a) and tan δ (b) values of the PBO fiber/m-BADCy wave-transparent laminated composites at different testing frequencies.

where d represents the thickness of wave-transparent laminated composites; λ represents the wavelength of the electromagnetic wave; θ represents the angle of incidence on the surface of wave-transparent laminated composites; and ε and tan δ represent the values for the dielectric constant and dielectric loss tangent of wave-transparent laminated composites, respectively.

The T values for the pristine PBO fiber/m-BADCy, PBO@lysozyme fiber/m-BADCy and f-PBO fiber/m-BADCy wave-transparent laminated composites were 93.2%, 93.4% and 93.6%, respectively. This revealed that the above wave-transparent laminated composites all presented excellent wave-transparent properties. Herein, f-PBO fiber/m-BADCy wave-transparent laminated composites possessed the optimal permeability. Fig. 8 shows the schematic diagram of the wave-transparent mechanisms for the PBO fiber/m-BADCy wave-transparent laminated composites.

3.3.2. Mechanical properties. Fig. 9 shows the interlaminar shear strength (ILSS) and flexural strength of the PBO fiber/m-BADCy wave-transparent laminated composites. Compared with those of pristine PBO fiber/m-BADCy and PBO@lysozyme fiber/m-BADCy wave-transparent laminated composites, the f-PBO fiber/m-BADCy wave-transparent laminated composites possessed the maximum ILSS (47.6 MPa) and flexural strength (805.8 MPa), increased by 23.0% and 33.5% in comparison to those of pristine PBO fiber/m-BADCy wave-transparent laminated composites (ILSS = 38.7 MPa and flexural strength = 603.5 MPa), respectively. The reason was that some active groups (amino and carboxyl groups, *etc.*) were introduced on the surface

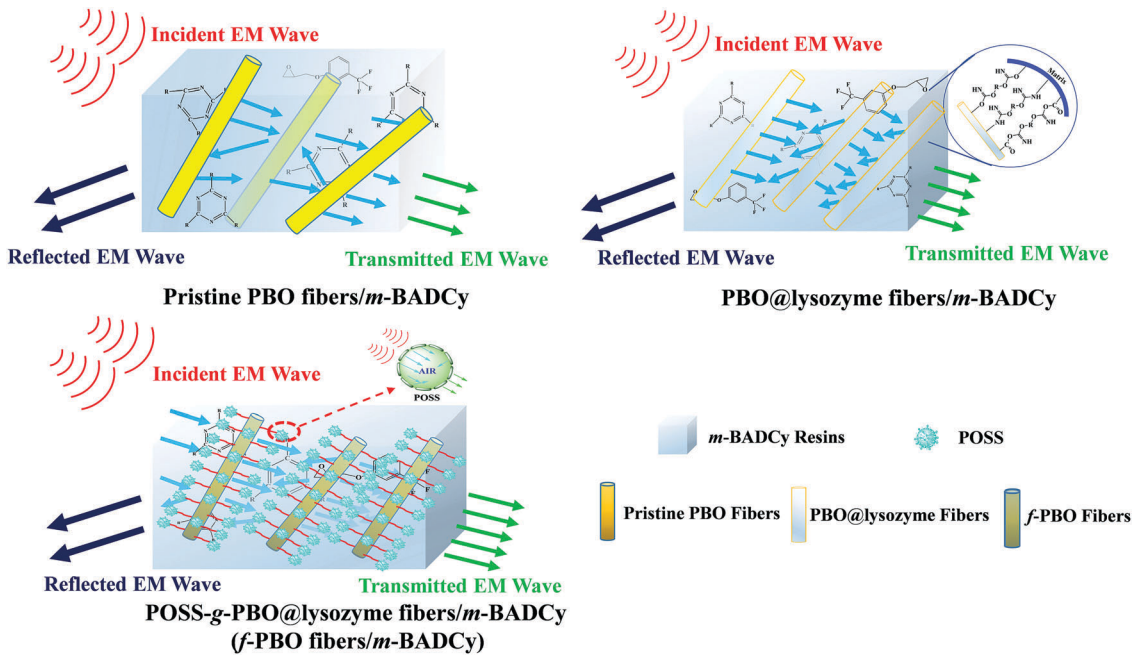

Fig. 8 Schematic diagram of the wave-transparent mechanisms for the PBO fiber/m-BADCy wave-transparent laminated composites.

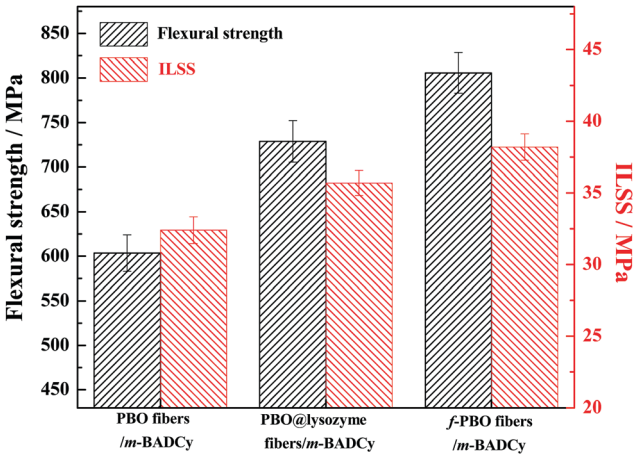

Fig. 9 Interlaminar shear strength (ILSS) and flexural strength of the PBO fiber/m-BADCy wave-transparent laminated composites.

Table 3 Volume fraction of pristine and functionalized PBO fibers (V_f) and the coefficient of dispersion

Samples	V_f	
	Average value/%	Coefficient of dispersion/%
Pristine PBO fibers/m-BADCy	43.59	1.94
PBO@lysozyme fibers/m-BADCy	40.34	0.95
f-PBO fibers/m-BADCy	39.07	0.75

for PBO@lysozyme fibers, in favor of improving the interfacial compatibility between PBO@lysozyme fibers and the m-BADCy matrix. Furthermore, with the incorporation of POSS, a large number of hydroxyl groups were also introduced on the surface for the f-PBO fibers, and participated in the curing reaction of the m-BADCy resin, which were also beneficial to decrease the inner defects and gaps in the composite system. In addition, POSS can form a good inorganic/organic hybrid system with the m-BADCy matrix, which further improves the mechanical properties of the f-PBO fiber/m-BADCy wave-transparent laminated composites accordingly. The corresponding gel content (or volume fraction of PBO fibers, V_f) values of the above three laminated composites (Table 3) further demonstrate the improved interfacial compatibility of the functionalized PBO fibers with the m-BADCy matrix.

3.3.3. Thermal properties. Fig. 10 shows the TGA curves of the PBO fiber/m-BADCy wave-transparent laminated composites. The corresponding characteristic thermal data are summarized in Table 4. The weight loss of the pristine PBO fiber/m-BADCy wave-transparent laminated composites prior to 100 °C was less than 1%, which was mainly attributed to the evaporation of small molecules. The corresponding weight loss increased to 30.6% at 600 °C, owing to the cracking, even the decomposition, of main chains for the m-BADCy matrix. The final mass of residual was 50.7% at 900 °C, which was mainly ascribed to the char and decomposition of the PBO fibers at relatively higher temperatures.[69] At the same weight loss, the thermal decomposition temperatures and $T_{\text{heat-resistance index}}$ (T_{HRI})[70] values of the PBO@lysozyme fiber/m-BADCy and f-PBO fiber/m-BADCy wave-transparent laminated composites were both lower than those of pristine PBO fiber/m-BADCy wave-transparent laminated composites. Meantime, the T_{HRI} value of the f-PBO fiber/m-BADCy wave-transparent laminated composites was 228.3 °C, slightly higher than that of PBO@lysozyme fiber/m-BADCy wave-transparent laminated composites (T_{HRI} = 226.3 °C). The reason was that lysozyme and POSS could be oxidized or pyrolyzed at higher temperatures. POSS presented a relatively better thermal stability than lysozyme.

The corresponding T_g value of the PBO@lysozyme fiber/m-BADCy and f-PBO fiber/m-BADCy wave-transparent laminated composites was 233.9 and 252.1 °C, increased by 29.2 and 47.4 °C, respectively, compared to that of pristine PBO fiber/m-BADCy wave-transparent laminated composites (T_g = 204.7 °C). This indicated that the surface functionalization of PBO fibers would further improve the T_g values of the wave-transparent laminated composites. On one hand, active groups on the surface of PBO@lysozyme and f-PBO fibers were both increased, resulting in more stable interfacial action and higher T_g values. On the

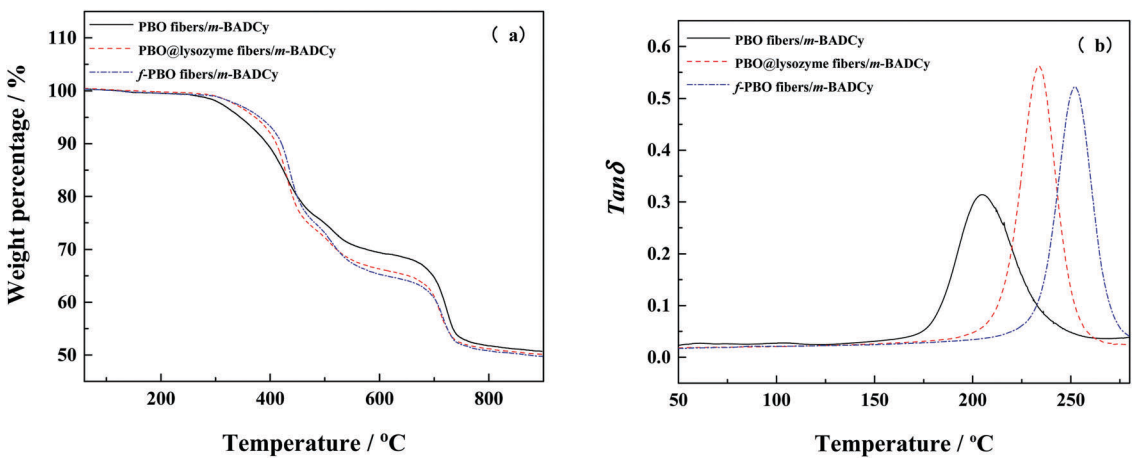

Fig. 10 TGA (a) and DMA (b) curves of the PBO fiber/m-BADCy wave-transparent laminated composites.

Table 4 Characteristic thermal data of the PBO fiber/m-BADCy wave-transparent laminated composites

Samples	Weight loss temperature/°C				
	T_5	T_{30}	T_{50}	$T_{\text{heat-resistance index}}$[a]/°C	T_g/°C
PBO fibers/m-BADCy	345.2	576.6	—	236.6	204.7
PBO@lysozyme fibers/m-BADCy	372.2	521.5	—	226.3	233.9
f-PBO fibers/m-BADCy	381.1	522.5	869.1	228.3	252.1

[a] The sample's heat-resistance index[70] is calculated with eqn (4).

$$T_{\text{Heat-resistance index}} = 0.49 \times [T_5 + 0.6 \times (T_{30} - T_5)] \quad (4)$$

where T_5 and T_{30} are the corresponding decomposition temperatures for 5% and 30% weight loss, respectively.

other hand, POSS might form chemical & physical entanglement with the m-BADCy matrix, further enhancing the interfacial bonding between f-PBO fibers and the m-BADCy matrix, resulting in a relatively higher T_g value.

4. Conclusions

FTIR, XPS, TGA and SEM analyses revealed that lysozyme was coated on the surface of PBO fibers and POSS was also successfully grafted onto the PBO@lysozyme fibers. Compared with that of pristine PBO fiber/m-BADCy micro-composites, the corresponding single fiber pull-out strength of PBO@lysozyme fiber/m-BADCy and f-PBO fiber/m-BADCy micro-composites increased from 3.21 to 3.73 and 4.00 MPa, respectively. The obtained f-PBO fiber/m-BADCy wave-transparent laminated composites presented more excellent dielectric & mechanical properties, and also possessed outstanding thermal stability. And the corresponding ε and $\tan\delta$ values at 10^7 Hz decreased to 2.81 and 0.0028, reduced by 3.4% and 34.9% in comparison to those of pristine PBO fiber/m-BADCy laminated composites (ε = 2.91 and $\tan\delta$ = 0.0043), respectively. The interlaminar shear strength (ILSS) and flexural strength of the f-PBO fiber/m-BADCy wave-transparent laminated composites increased to 47.6 and 805.8 MPa, increased by 23.0% and 33.5% in comparison to those of PBO fiber/m-BADCy wave-transparent laminated composites (ILSS = 38.7 MPa and flexural strength = 603.5 MPa), respectively. In addition, the T_{HRI} and T_g values of the f-PBO fiber/m-BADCy wave-transparent laminated composites were 228.3 and 252.1 °C, respectively. These f-PBO fiber/m-BADCy wave-transparent laminated composites present promising applications in radomes and antenna systems of aircrafts.

Conflicts of interest

There are no conflicts to declare.

Acknowledgements

The authors are grateful for the support and funding from the Foundation of National Natural Science Foundation of China (No. 51773169); Space Supporting Fund from China Aerospace Science and Industry Corporation (No. 2017-HT-XG); Aeronautics Science Fund (No. 2016ZF03010, 2015ZF53071 and 2015ZF53074); Fundamental Research Funds for the Central Universities (No. 3102017jg02003); Y. Li thanks the Seed Foundation of Innovation and Creation for Graduate Students in NPU (No. ZZ2018034); Y. K. Zhang thanks the Undergraduate Innovation & Business Program in NPU. We would like to thank the Analytical & Testing Center of Northwestern Polytechnical University for testing and characterization.

References

1 (*a*) B. Smith, T. Schäffer, M. Viani, J. Thompson, N. Frederick, J. Kindt, A. Belcher, G. Stucky, D. Morse and P. Hansma, *Nature*, 1999, **399**, 761–763; (*b*) Z. Wu, H. Cui, L. Chen, D. Jiang, L. Weng, Y. Ma, X. Li, X. Zhang, H. Liu, N. Wang, J. Zhang, Y. Ma, M. Zhang, Y. Huang and Z. Guo, *Compos. Sci. Technol.*, 2018, **164**, 195–203.
2 Y. Tang, W. Dong, L. Tang, Y. Zhang, J. Kong and J. Gu, *Compos. Commun.*, 2018, **8**, 36–41.
3 K. Pickering, M. Efendy and T. Le, *Composites, Part A*, 2016, **83**, 98–112.
4 Y. Li, X. Yi, T. Yu and G. Xian, *Adv. Compos. Hybrid Mater.*, 2018, **1**, 231–246.
5 H. Zhao, L. Chen, J. Yun, L. Tang, Z. Wen, X. Zhang and J. Gu, *Eng. Sci.*, 2018, **2**, 57–66.
6 X. Zhou and G. Hu, *Phys. Rev. E: Stat., Nonlinear, Soft Matter Phys.*, 2006, **74**, 026607.
7 J. Karger-Kocsis, H. Mahmood and A. Pegoretti, *Prog. Mater. Sci.*, 2015, **73**, 1–43.
8 J. Gu, W. Dong, S. Xu, Y. Tang, L. Ye and J. Kong, *Compos. Sci. Technol.*, 2017, **144**, 185–192.
9 W. Qin, F. Vautard, L. Drzal and J. Yu, *Composites, Part B*, 2015, **69**, 335–341.
10 J. Thomason, *Composites, Part A*, 2009, **40**, 114–124.
11 Y. Tang, J. Gu, Y. Yu and J. Kong, *Polym. Compos.*, 2015, **36**, 2017–2021.
12 Z. Hou, X. Tian, J. Zhang and D. Li, *Compos. Struct.*, 2018, **184**, 1005–1010.
13 (*a*) B. Yu, X. Li, J. An, Z. Jiang and J. Yang, *Eng. Sci.*, 2018, **2**, 67–73; (*b*) C. Wang, M. Zhao, J. Li, J. Yu, S. Sun, S. Ge, X. Guo, F. Xie, B. Jiang, E. Wujcik, Y. Huang, N. Wang and Z. Guo, *Polymer*, 2017, **131**, 263–271; (*c*) M. Zhao, L. Meng, L. Ma, L. Ma, X. Yang, Y. Huang, J. E. Ryu, A. Shankar, T. Li, C. Yan and Z. Guo, *Compos. Sci. Technol.*, 2018, **154**, 28–36.
14 B. Guo, L. Wang, P. Yin, B. Li and P. Li, *J. Thermoplast. Compos. Mater.*, 2017, **30**, 564–577.
15 O. Haupt, K. Linnow, R. Harmel, C. Schaefer and W. Dannecker, *X-Ray Spectrom.*, 2015, **26**, 79–84.
16 B. Zhao, C. Zhao, C. Wang and C. Park, *J. Mater. Chem. C*, 2018, **6**, 3065–3073.

17 Y. Tang, J. Gu and T. Bai, *Fibers Polym.*, 2012, **13**, 1249.
18 L. Chen, Y. Du, Y. Huang, F. Wu, H. Cheng, B. Fei and J. Xin, *Composites, Part A*, 2016, **88**, 123–130.
19 J. Gu, T. Bai, J. Dang, J. Feng and Q. Zhang, *Polym. Compos.*, 2014, **35**, 611–616.
20 P. Zhu, B. Liu and L. Bao, *Prog. Org. Coat.*, 2018, **116**, 43–50.
21 E. Mäder, S. Melcher, J. Liu, S. Gao, A. Bianchi, S. Zherlitsyn and J. Wosnitza, *J. Mater. Sci.*, 2007, **42**, 8047–8052.
22 D. Liu, P. Chen, J. Mu, Q. Yu and C. Lu, *Appl. Surf. Sci.*, 2011, **257**, 6935–6940.
23 L. Chen, Y. Du, Y. Huang, P. Ng and B. Fei, *Compos. Sci. Technol.*, 2016, **129**, 86–92.
24 I. Ahmad, R. Ismail and I. Abdullah, *Polym. Eng. Sci.*, 2011, **51**, 419–425.
25 Y. Xu, J. Zhu, Z. Wu, Y. Cao, Y. Zhao and W. Zhang, *Adv. Compos. Hybrid Mater.*, 2018, DOI: 10.1007/s42114-018-0032-7.
26 K. Tamargo-Martínez, A. Martínez-Alonso, M. Montes-Morán and J. Tascón, *Compos. Sci. Technol.*, 2011, **71**, 784–790.
27 G. Wu, Y. Shyng, S. Kung and C. Wu, *Vacuum*, 2009, **83**, S271–S274.
28 L. Chen, C. Wang, Z. Wu, G. Wu and Y. Huang, *Polym. Degrad. Stab.*, 2016, **133**, 275–282.
29 C. Zhang, Y. Huang and Y. Zhao, *Mater. Chem. Phys.*, 2005, **92**, 245–250.
30 G. Wu and Y. Shyng, *Composites, Part A*, 2004, **35**, 1291–1300.
31 G. Wu and Y. Shyng, *J. Polym. Res.*, 2005, **12**, 93–102.
32 L. Chen, F. Wei, L. Liu, W. Cheng, Z. Hu, G. Wu, Y. Du, C. Zhang and Y. Huang, *Compos. Sci. Technol.*, 2015, **106**, 32–38.
33 L. Chen, Y. Du, Y. Huang, F. Wu, H. Cheng, B. Fei and J. Xin, *Composites, Part A*, 2016, **88**, 123–130.
34 D. Liu, P. Chen, M. Chen and Z. Liu, *Surf. Coat. Technol.*, 2012, **206**, 3534–3541.
35 A. Jung, A. Sippel, M. Grez and G. Schütz, *Proc. Natl. Acad. Sci. U. S. A.*, 1980, **77**, 5759–5763.
36 S. Yuan, D. Wan, B. Liang, S. Pehkonen, Y. Ting, K. Neoh and E. Kang, *Langmuir*, 2011, **27**, 2761–2774.
37 Y. Liu, L. Porcar, J. Chen, W. Chen, P. Falus, A. Faraone, E. Fratini, K. Hong and P. Baglioni, *J. Phys. Chem. B*, 2011, **115**, 7238.
38 X. Zhong, Y. Song, P. Yang, Y. Wang, S. Jiang, X. Zhang and C. Li, *PLoS One*, 2016, **11**, e0146957.
39 M. d'Ischia, A. Napolitano, V. Ball, C. Chen and M. Buehler, *Acc. Chem. Res.*, 2014, **47**, 3541–3550.
40 Q. Ye, F. Zhou and W. Liu, *Chem. Soc. Rev.*, 2011, **40**, 4244–4258.
41 D. Wang, Y. Ha, J. Gu, Q. Li, L. Zhang and P. Yang, *Adv. Mater.*, 2016, **28**, 7414–7423.
42 A. Gao, Q. Wu, D. Wang, Y. Ha, Z. Chen and P. Yang, *Adv. Mater.*, 2016, **28**, 579–587.
43 X. Yang, L. Tang, Y. Guo, C. Liang, Q. Zhang, K. Kou and J. Gu, *Composites, Part A*, 2017, **101**, 237–242.
44 K. Suenaga, K. Tanaka and Y. Chujo, *Chem. – Eur. J.*, 2017, **23**, 1409–1414.
45 K. Raftopoulos and K. Pielichowski, *Prog. Polym. Sci.*, 2016, **52**, 136–187.
46 J. Liu, H. Yu, Q. Liang, Y. Liu, J. Shen and Q. Bai, *J. Colloid Interface Sci.*, 2017, **497**, 402–412.
47 X. Yang, Y. Guo, X. Luo, N. Zheng, T. Ma, J. Tan, C. Li, Q. Zhang and J. Gu, *Compos. Sci. Technol.*, 2018, **164**, 59–64.
48 (*a*) H. Kang, Q. Shao, X. Guo, A. Galaska, Y. Liu and Z. Guo, *Eng. Sci.*, 2018, **1**, 78–85; (*b*) Z. Wu, S. Gao, L. Chen, D. Jiang, Q. Shao, B. Zhang, Z. Zhai, C. Wang, M. Zhao, Y. Ma, X. Zhang, L. Weng, M. Zhang and Z. Guo, *Macromol. Chem. Phys.*, 2017, **218**, 1700357; (*c*) M. Xia, H. Yang, J. Ling, Q. Yao, G. Li and Y. Luo, *Adv. Compos. Hybrid Mater.*, 2018, **1**, 310–319.
49 S. Jian, C. Ding, T. Yang, C. Zhang and H. Hou, *Compos. Commun.*, 2018, **7**, 42–46.
50 X. Yang, C. Liang, T. Ma, Y. Guo, J. Kong, J. Gu, M. Chen and J. Zhu, *Adv. Compos. Hybrid Mater.*, 2018, **1**, 207–230.
51 Y. Wang, L. Chen, T. Xu, Y. Yan, J. Gu and J. Yun, *Polym. Degrad. Stab.*, 2017, **137**, 184–196.
52 S. Wang, S. Dong, Y. Gao and Y. Sun, *Mater. Des.*, 2017, **115**, 213–223.
53 P. Chang, C. Tian, K. Chen, S. Liang, J. Qing, Y. Zhu, X. Jia and J. Wang, *High Perform. Polym.*, 2016, **28**, 119–128.
54 Y. Li, G. Xu, Y. Guo, T. Ma, X. Zhong, Q. Zhang and J. Gu, *Composites, Part A*, 2018, **107**, 570–578.
55 Q. Li, X. Wang and H. Yan, *Polym. Bull.*, 2016, **73**, 2343–2352.
56 W. Ling, A. Gu, G. Liang and L. Yuan, *Polym. Compos.*, 2010, **31**, 307–313.
57 J. Gu, S. Xu, Q. Zhuang, Y. Tang and J. Kong, *IEEE Trans. Dielectr. Electr. Insul.*, 2017, **24**, 784–790.
58 Y. Shen, A. Gu, G. Liang and L. Yuan, *Composites, Part A*, 2010, **41**, 1668–1676.
59 M. Zhang, H. Yan, X. Yang and C. Liu, *RSC Adv.*, 2016, **6**, 38887–38896.
60 X. Zhan, L. Wang, J. Zhang and J. Cheng, *Mater. Des.*, 2015, **88**, 1100–1108.
61 Y. Mi, G. Liang, A. Gu, F. Zhao and L. Yuan, *Ind. Eng. Chem. Res.*, 2013, **52**, 3342–3353.
62 P. Ren, G. Liang and Z. Zhang, *Polym. Compos.*, 2006, **27**, 402–409.
63 Z. Zhao, R. Guan, J. Zhang, Z. Zhao and P. Bai, *Acta Metall. Sin.*, 2017, **30**, 66–72.
64 G. Liang and M. Zhang, *J. Appl. Polym. Sci.*, 2002, **85**, 2377–2381.
65 J. Gu, W. Dong, Y. Tang, Y. Guo, L. Tang and J. Kong, *J. Mater. Chem. C*, 2017, **5**, 6929–6936.
66 Q. Ma, B. Wang, J. Lv, H. Li, B. Lei and C. Zhao, *Mater. Lett.*, 2017, **202**, 52–54.
67 J. T. Kindt and C. A. Schmuttenmaer, *J. Phys. Chem. C*, 1996, **100**, 10373–10379.
68 W. Xia, Y. Han, J. Yang and H. Xie, *Hi-Tech Fiber Appl.*, 2003, **25**, 40–43.
69 Z. Hu, Q. Shao, Y. Huang, L. Yu, D. Zhang, X. Xu, J. Lin, H. Liu and Z. Guo, *Nanotechnology*, 2018, **29**, 185602.
70 Y. Guo, G. Xu, X. Yang, K. Ruan, T. Ma, Q. Zhang, J. Gu, Y. Wu, H. Liu and Z. Guo, *J. Mater. Chem. C*, 2018, **6**, 3004–3015.

